Annu. Rev. Biophys. Biomol. Struct. 1996. 25:395–429

VISUALIZING PROTEIN–NUCLEIC ACID INTERACTIONS ON A LARGE SCALE WITH THE SCANNING FORCE MICROSCOPE

Carlos Bustamante and Claudio Rivetti*

Institute of Molecular Biology and *Howard Hughes Medical Institute, University of Oregon, Eugene, Oregon 97403

KEY WORDS: scanning force microscopy, protein-induced DNA bending

ABSTRACT

CONTENTS

PROSPECTIVES AND OVERVIEW

Until recently, the electron microscope (EM) was the only tool available to characterize the study of the large-scale spatial relationships of nu-

1056-8700/96/0610-0395$08.00

cleoprotein assemblies. This situation has changed rapidly in the last 3 years, as several groups have demonstrated the feasibility of using the scanning force microscope (SFM) to investigate these complex biological systems. With capabilities often complementary to those of the EM, the SFM is becoming a useful tool of structural characterization of protein–nucleic acid complexes and their interactions in air and in aqueous solutions.

The last 15 years have witnessed the extraordinary growth of structural studies in biology, and the impact is being felt in almost all areas of biological research. This growth reflects not only the use of improved analytical methods in biochemistry but also the coming of age of the two most powerful techniques of high-resolution structural determination: X-ray crystallography and NMR. In contrast, the tools available to the biochemist at the next higher level of biomolecular organization are significantly more limited. Because this regime comprises objects with dimensions between 10 and 200 nm, it has been termed ''mesoscopic''; the structures are often too complex for X-ray or NMR analysis and, yet, too small to be seen with the optical microscope. For decades, the EM has been the only analytical tool for this structural regime. Despite the power and versatility of the EM, scientists have welcomed the development of alternative methods that can analyze mesoscopic structures under conditions more closely resembling their physiologic environment.

The study of protein–nucleic acid complexes is paradigmatic of this situation. Several nucleic acid binding proteins have been solved at atomic resolution, and their number is increasing rapidly. A much smaller number of high-resolution structures of protein–nucleic acid complexes exist, and their number is increasing at a slower rate. This scenario worsens at the next level of complexity, which involves large multimolecular assemblies that participate in the regulation of transcription and replication.

The invention in 1986 of the SFM (6), also called atomic force microscope, has equipped biologists with a powerful new tool of structural characterization of protein–nucleic acid interactions. In this article, we review the use of SFM to investigate nucleoprotein assemblies of a broad range of dimensions and complexity. Although we include structural studies of chromatin, we exclude studies of the higher order organization of metaphase and polytene chromosomes; their unique requirements of sample preparation and deposition set them apart from the nucleoprotein assemblies considered here. Because of the novelty of these applications, we emphasize several technical aspects of sample preparation and deposition.

THE SCANNING FORCE MICROSCOPE

The SFM is a member of a new class of high-resolution microscopes known generically as scanning probe microscopes. These instruments do not use lenses to form an image but, instead, use a sharply pointed sensor, or "tip," to probe the surface of the sample. In the SFM, the tip is mounted on the end of a flexible cantilever (Figure 1). As the sample is scanned beneath the tip, small forces of interaction with the

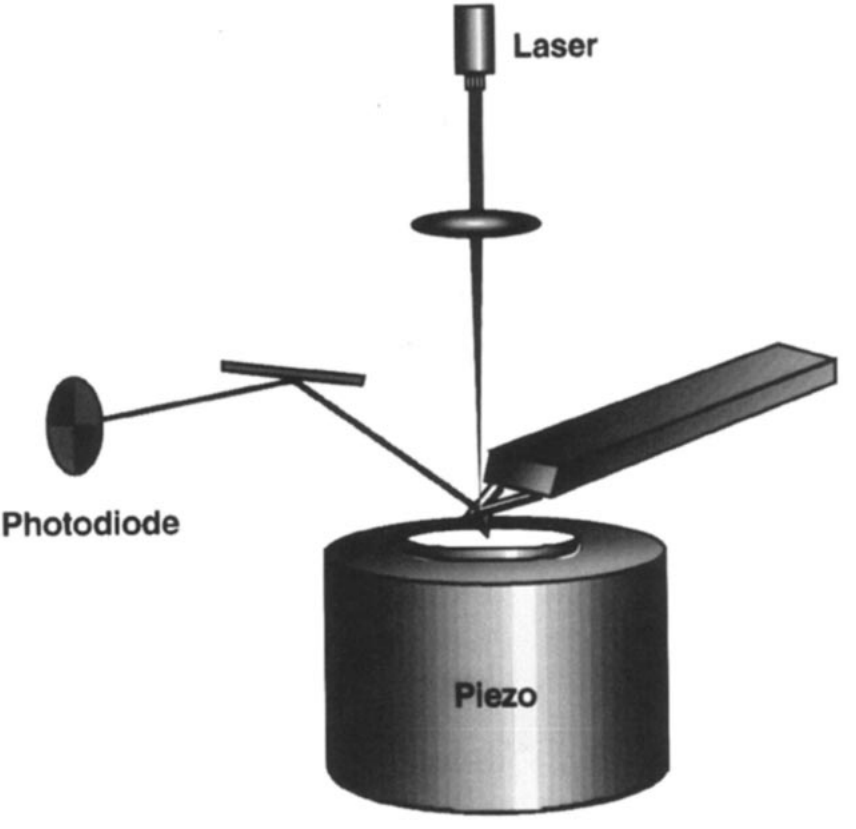

Figure 1 Schematic view of an SFM microscope. The sample is placed on the piezoelectric driver and scanned relative to the tip. In contact mode operation, the surface topography can be obtained directly from the deflection of the cantilever, detected by using the deflection of a laser beam reflected off the back of the cantilever onto a four-quadrant photo diode (optical lever system). Alternatively, the optical lever can be used with a feedback circuit to raise or lower the sample as it is scanned under the tip to cancel the deflection of the cantilever. The image is obtained by converting the voltage applied to the piezo into height information.

sample cause the cantilever to deflect, thereby revealing the sample topography. Deflections as small as 0.01 nm can be detected simply by directing a laser beam on the back of the cantilever and monitoring the amplified deflection of the reflected beam with a four-quadrant photodiode (see 64, 65). The biological applications of this method also have been reviewed recently (9–11, 28).

One of the most attractive features of the SFM is that it can operate at least as well with the cantilever immersed in liquid as in air, which makes it possible to image biological molecules in aqueous buffers. The SFM is, therefore, the first (and so far only) microscope that can achieve nanometer scale resolution on biological samples under physiologic conditions.

Modes of Operation

The SFM can be operated in three different modes: contact, noncontact, and tapping. We consider only contact and tapping applications here, because no biological applications of the noncontact mode have been described to date. In contact mode, the tip is continuously in contact with the surface as it slides over the sample. This operation usually yields stable images, but compression and shear forces generated between the tip and surface may damage the sample. Typical operation forces in contact mode are 1–10 nN. In tapping mode, the cantilever is oscillated up and down at hundreds of kiloHertz as it is scanned relatively to the sample; thus, the tip is allowed to make transient contact with the sample at the bottom of its swing. Because the tip touches the sample, the resolution is usually almost as good as in contact mode. Because the contact is very brief, however, the damage caused by shear forces during scanning is reduced greatly. Imaging of nucleoprotein complexes in air is easier and more reliable in tapping mode than in contact mode.

The tapping mode has been adapted recently for imaging in liquids (29, 60, 61), and its applications to biological molecules in aqueous environments are increasing rapidly. Tapping mode imaging in liquid has several advantages over both the contact mode and the tapping mode in air (9, 29, 60, 61). Tapping in liquid eliminates the liquid–air interface, thereby reducing the capillary forces between the tip and the sample (see below). This feature makes it possible to decrease the amplitude of oscillation of the cantilever without it being captured by the attractive forces. Smaller oscillation amplitudes lead, in turn, to better control of the force acting on the sample and to reduced sample damage (10). Moreover, the smaller shearing forces developed in tapping make stable imaging in liquids possible, as biological samples can

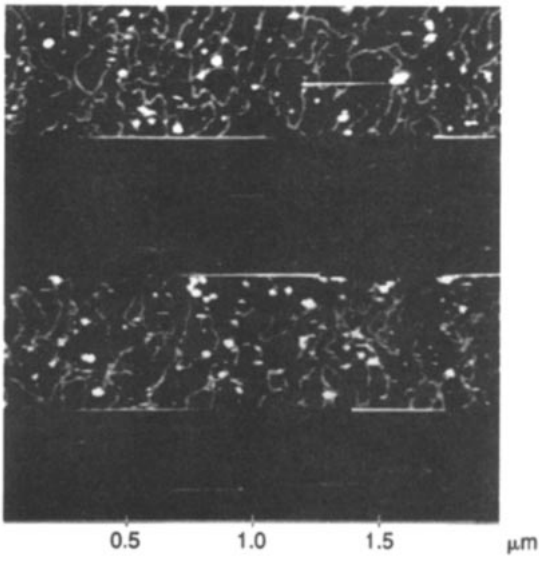

Figure 2 Image of a 1200-bp DNA fragment in buffer (40 mM Tris pH 7.5, 30 mM potassium acetate, 10 mM $MgCl_2$). The first and the third sectors were obtained with tapping mode AFM. In the second and the fourth sectors, the mode of operation was reverted to contact mode. The scan rate was 1.05 Hz, and the tapping frequency was 16.5 kHz. The mean height of the DNA in this image was approximately 1.4 nm. (Image courtesy of G Yang, Institute of Molecular Biology, University of Oregon.)

be detached easily from the surface when they are immersed in an aqueous solution. One example of this effect is illustrated in Figure 2, in which DNA fragments are imaged alternatively in tapping and contact modes. In contact mode, the molecules are swept by the tip, whereas they are imaged reliably in tapping mode.

Imaging of protein–nucleic acid complexes with the use of the tapping mode in liquid is not yet as reliable as in air, probably because of complex hydrodynamic interactions between the sample and the oscillating cantilever. This situation, however, is likely to change in the near future; it is the subject of much attention from several groups interested in visualizing protein–nucleic acid interactions as they occur in nearly physiologic conditions.

Spatial Resolution

The mechanism of image formation in the SFM is very different from those of optical and electron microscopes. The spatial resolution of optical and electron microscopes is a property inherent to the instrument and dependent ultimately on the design and principles of operation of

the microscope. In contrast, the spatial resolution of the SFM depends as much on the characteristics of the sample as on the inherent properties of the instrument (10). Thus, although theories of image formation for probe microscopy exist (9, 33, 56), there is no general definition of resolution in force microscopy.

The most important instrument parameter affecting the spatial resolution in SFM is the sharpness of the tip (11), usually described in terms of its end-radius of curvature R_c. Tips with end radii of approximately 10 nm are fabricated easily (11, 32), and resolvable features in an SFM image are typically 5–10 nm apart.

Besides tip dimensions, whether two distinct features of a given object can be resolved depends on the context of each feature in the object (10). This idea is illustrated schematically in Figure 3, where two sharp spikes separated by a distance, *d,* are imaged by a parabolic tip with end-radius R_c. Because the sample is sharper than the tip, the image is the surface defined by the envelope of a pair of inverted tip profiles ''hanging'' on the spikes (33). The surface and volume of the resulting image is not the ''sum'' of the images of the individual spikes but rather the union of sets of inverted tip profiles, i.e. the imaging process in SFM is an inherently nonlinear process. In Figure 3*a,* the surface displays a small dimple between the spikes of depth, Δz, which is determined by the tip shape and size and the separation between the spikes. One definition of ''resolution'' is, then, the minimum separation d for which the dimple depth Δz is significantly larger than the instrumental noise. This definition is the closest analogue to the Rayleigh resolution criterion in optical microscopy. The difficulty with this simple idea, however, is shown in Figure 3*b:* As the height difference between the two spikes increases, the depth of the dimple decreases. Two objects that are ''resolved'' when their heights are nearly equal, therefore, may not be resolved when their heights are unequal. This example shows that resolution in force microscopy is also a function of the height difference Δh between adjacent features and must be determined independently for each feature in the object.

Using the definition of resolution in the preceding paragraph, the minimum separation, d, that will result in a dimple of depth Δz for spikes with height difference Δh imaged by a parabolic tip is given by (10):

$$d = \sqrt{2R_c}\left(\sqrt{\Delta z} + \sqrt{\Delta z + \Delta h}\right) \quad \text{for } d > \sqrt{2R_c \Delta h}. \qquad 1.$$

For features of equal height, and using a parabolic tip with $R_c = 10$ nm, a detectable dimple depth of 0.5 nm yields a minimum resolved

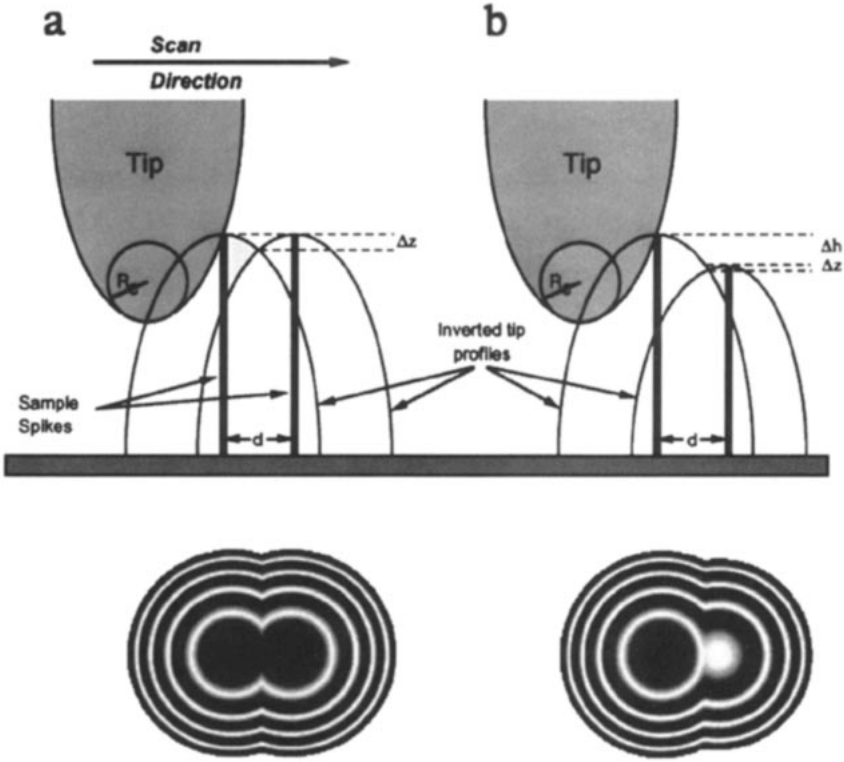

Figure 3 Schematic diagram of the factors that determine the spatial resolution in SFM. Two spikes separated by a distance d are imaged by a parabolic tip with end radius R_c. *(a)* The two spikes have the same height and are well resolved in the image that shows a dimple Δz in between the maxima. *(b)* As the difference in height between the two spikes increases, the resolution decreases (Δz becomes smaller), even though the spikes separation remains constant. Contour plots of the images of the two spikes obtained by the tip in each case are shown below.

separation $d = 6.4$ nm. By comparison, if the height difference is 2.0 nm, the minimum resolved separation is 12.5 nm. This analysis assumes perfectly rigid surfaces for the tip and the sample. In practice, a given feature may be resolved better or worse than this estimate because of sample compliance.

Tip-Sample Interactions

One of the main concerns in the applications of the SFM to study biological structures in general, and protein–nucleic acid assemblies

in particular, is the effect of tip-sample forces. Several forces are present between the tip and the sample during imaging (64). Their effect on the sample and on the resulting image depends on their magnitude, the SFM mode of operation, the imaging environment, the nature of the sample, and the sharpness, composition, and shape of the tip (11).

In air, capillary forces and hard-core repulsions between tip and sample are dominant (10). Capillary forces play a major role when imaging in air because, under normal ambient conditions, all samples have a thin layer of water on their surface. Even a few monolayers of adsorbed water can give rise to a water meniscus between the surface and the tip. The resulting attractive force is often strong enough to pin the tip to the surface (11, 13, 64, 77). This force, known as Laplace's force (31), can be as large as a few hundred nN but can be reduced to 1–10 nN by controlling the ambient humidity. Typically, protein–nucleic acid complexes can be imaged reliably in air with a relative humidity of less than 35%, and the samples can be scanned several times without noticeable damage (11, 13, 77, 80). At greater humidity, imaging in contact mode is not stable, because the complexes are swept easily by the tip, unless special care has been taken to strengthen the sample–surface interaction. In contact mode, this component of the total capillary force puts a limit on the lowest imaging tip–sample force and, hence, on the minimum damage to the sample and to the tip. In tapping mode, the molecules are not swept by the tip even at high levels of humidity, but the resulting capillary forces put a lower limit on the amplitude of oscillation required to prevent capture of the oscillating tip by the liquid meniscus and, thus, to determine the minimum operational tip-sample force (9).

Imaging in liquids eliminates the liquid–air interface, thereby reducing the attractive capillary forces greatly. In this case, tip–sample interactions are dominated by van der Waals and electrostatic forces in the range of 0.1 to 1 nN. As illustrated in Figure 2, however, even at these reduced forces, when imaging in contact mode the shear component of the tip–sample interaction may be sufficient to sweep the molecules off the surface.

Attractive forces are balanced by hard-core repulsions between the atoms of the sample and the atoms of the tip (31). If tip and sample are hard, this repulsion defines the sample surface effectively. If the sample is soft and the tip is sharp, however, the pressure caused by the attractive forces can deform or damage the sample. When imaging biological samples, a special effort should be made, therefore, to operate the microscope at the lowest level of possible forces.

SAMPLE PREPARATION AND DEPOSITION

Sample Preparation

Protocols for preparing protein–nucleic acid complexes that are suitable for SFM studies are similar to those used in bulk biochemical studies, but better images are often obtained when the complexes are deposited on the substrate in low salt buffer (<100 mM). Samples that require high salt conditions for the binding reaction (100–500 mM), should be diluted before deposition on the substrate to minimize the formation of salt microcrystals during the drying step. Deposition buffers commonly used are Tris, Hepes, and triethanolamine, with concentrations up to 100 mM of monovalent ions and 1–10 mM of divalent cations, such as Mg^{++}, Mn^{++}, Co^{++}, and Ca^{++}.

Sample purity is essential to obtain reliable imaging with the SFM. Double distilled water and, if possible, nanopure water should be used in the preparation steps. In particular, DNA samples must be purified of contaminating proteins carefully; highly purified proteins are desirable, and protein stabilizers, such as bovine serum albumen (BSA) or glycerol, should be avoided to prevent contamination of the background.

Deposition Protocols

Development of reliable protocols of DNA deposition for SFM have received much attention in the last 4 years. Most of these protocols have not been used with protein–nucleic acid complexes. If the adhesion to the substrate is dominated by the nucleic acid, however, these protocols, with minor modifications, probably could be adapted to image protein–nucleic acid complexes.

The most commonly used substrate has been freshly cleaved mica. The presence of a divalent cation, such as Mg^{++}, in the deposition buffer increases the adhesion of DNA and protein–nucleic acid complexes to the surface greatly (13, 76, 80, 89). Freshly cleaved mica is negatively charged (53); Mg^{++} appears to promote DNA deposition by binding to the mica surface and inverting its charge (11). Increased DNA binding can be obtained also by glow discharging the mica surface before the deposition of the DNA molecules. Other methods of deposition require treating the mica with aminopropyltrimethoxy silane (42, 43, 45); carbon coatings (87); nonionic detergents, such as 2, 4, 6-tris-(dimethylaminomethyl) phenol; cationic detergents, like cetylpyridinium chloride (67); or benzyldimethylalkylamonium chloride (66). Replica methods also have been used recently (14). DNA molecules depos-

ited on mica were overcoated with carbon, and the underside of the carbon layer was imaged in propanol after it was pealed off the mica.

A deposition protocol for imaging DNA molecules and protein–nucleic acid complexes in air involves the following steps: (*a*) placing the sample drop on the freshly cleaved mica; (*b*) allowing the molecules to bind for a deposition time of 1–2 min; (*c*) blotting the excess liquid; (*d*) rinsing with nanopure water; and (*e*) drying the sample under dry N_2 flow.

DEPOSITION KINETICS A recent study has shown that, in good deposition conditions (low salt buffer on mica), the transfer of DNA molecules from solution to the substrate is governed solely by diffusion (C Rivetti, M Guthold, and C Bustamante, in preparation). These authors showed that the density of DNA molecules deposited on mica can be described by the expression:

$$\frac{N^\circ \text{ DNA molecules}}{\text{Area}} = \frac{2}{\pi}[\text{DNA}]\sqrt{Dt}, \qquad 2.$$

where D is the diffusion coefficient of the DNA molecules, [DNA] is the number of DNA molecules/cm^3 in the deposition drop, and t is the time of deposition. Optimal deposition densities of DNA molecules on freshly cleaved mica are obtained at low salt conditions, with DNA concentrations of 0.5–2 nM, and deposition times of 1–2 min. For example, a 0.5-nM solution of DNA in 10 mM NaCl, 2 mM $MgCl_2$, and 4 mM Hepes buffer pH = 7.4 yields an average deposition density of approximately 5300 base pairs (bp)/μm^2 in a deposition time of 30 s and approximately 10,800 bp/μm^2 in 2 min (C Rivetti, M Guthold, and C Bustamante, in preparation). These deposition densities are also ideal for protein–nucleic acid complexes, although, as discussed below, the conditions of deposition must consider the stability and life time of the complexes to prevent complex dissociation.

MOLECULAR MECHANISMS OF DEPOSITION: EQUILIBRATION VS KINETIC TRAPPING Sample deposition and transfer of structures from three-dimensional space onto a two-dimensional surface can potentially alter the spatial relationships between the DNA fragment and its associated proteins, thereby preventing any quantitative characterization of the images. Little is known about the molecular mechanisms of this transfer process and the binding of the complexes to the surface. We present a first approximation here after we discuss the approach of two recent SFM studies conducted on DNA fragments (C Rivetti, M Guthold,

and C Bustamante, in preparation) and various protein–nucleic acid complexes (C Walker, WA Rees, DA Erie, and C Bustamante, in preparation).

The outcome of the deposition of nucleic acids or protein–nucleic acid complexes depends on the nature and strength of the molecule–surface interactions. Equilibration occurs if the molecules can approach the surface and search among their accessible states in two dimensions, before the blotting and drying steps. In this case, their appearance and dimensions are indistinguishable from an ensemble of molecules at equilibrium in two dimensions. Alternatively, kinetic trapping results if, during deposition, any segment of the molecules simply sticks to the surface and, thus, remain trapped at the contact sites. In this case, the molecular configurations reflect the history of their approach to the surface. Clearly, these two cases represent extreme alternatives. In practice, a particular deposition protocol may fall somewhere between these two extremes. Whether equilibration is attained may depend on the characteristic time required by the polymers to equilibrate on the surface, relative to the deposition time before blotting and drying. In turn, this characteristic time will depend on such factors as the polymer size, the strength of the molecule–surface interaction, and the number and distribution of the surface binding sites.

The time required by a polymer molecule to access its configurations when it is free to diffuse in two dimensions can be written as $t_0 \sim \nu^N / N\rho_0$, where N is the number of monomers in the polymer, ν is the degrees of freedom per monomer, and ρ_0 is the rate of transition of a monomer among its degrees of freedom. On the other hand, the equilibration time of a polymer molecule with a (steady-state) fraction f_b of its monomers interacting with binding sites on the surface can be written as:

$$t \sim \frac{t_0}{\left\{1 - f_b\left[1 - e\left(\frac{\Delta G_{bind}}{k_b T}\right)^{-1}\right]\right\}}, \qquad 3.$$

where T is the absolute temperature, k_B is the Boltzman's constant, and ΔG_{bind} is the binding energy of the molecule to each surface site. As indicated by Equation 3, the equilibration time of a polymer molecule that is partly bound to a surface increases with the size of the polymer, the binding energy to the surface, and the density of binding sites on the surface. In general, longer polymers require longer equilibration times before the blotting and drying steps of deposition.

Recently, Rivetti and colleagues addressed these issues (C Rivetti, M Guthold, and C Bustamante, in preparation). These authors compared

several deposition procedures of DNA on mica to determine whether the deposition process is dominated by equilibration or by kinetic trapping effects. To this end, DNA fragments of various lengths were deposited on freshly cleaved mica and allowed to equilibrate for 2 min at various ionic strength conditions and various Mg^{++} concentrations. The mean quadratic end-to-end distances of the molecules, $\langle R^2 \rangle$, were measured and compared with the equilibrium values predicted by the wormlike chain model (23) for molecules of the same contour length in two dimensions. According to this model,

$$\langle R^2 \rangle = 4PL\left[1 - \frac{P}{L}\left(1 - e^{-L/2P}\right)\right] \rightarrow 4PL \qquad \text{(for very large } L\text{)}, \qquad 4.$$

where P and L are the persistence length and the contour length of the DNA, respectively. Figure 4 compares $\langle R^2 \rangle$ values determined experi-

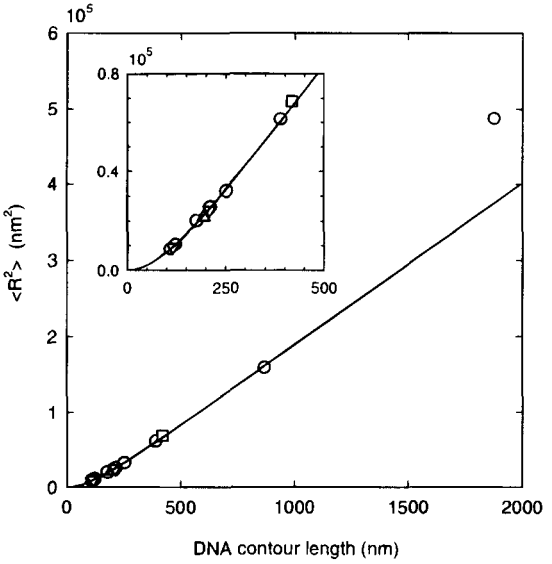

Figure 4 Plot of the mean square end-to-end distance, $\langle R^2 \rangle$, for various DNA sizes as a function of their contour length. The different symbols represent different buffer conditions: *circles*, 4 mM Hepes pH 7.4, 10 mM NaCl, 2 mM $MgCl_2$; *squares*, 4 mM Hepes pH 7.4, 10 mM NaCl, 100 mM $MgCl_2$; *triangles*, 10 mM Hepes pH 8.0, 80 mM NaCl, 5 mM $MgCl_2$; *inverted triangles*, 10 mM Hepes pH 6.8 and 8.0, 5 mM NaCl, 5 mM $MgCl_2$. The value corresponding to the longest DNA fragment (1877 nm) probably reflects the contribution of excluded volume effects. This value is an average of three different depositions in which different incubation times, ranging from 1 to 10 min, were used. The *solid line* is the $\langle R^2 \rangle$ predicted by the wormlike chain model (Equation 4), using a persistence length of 53 nm (12).

mentally for molecules in 4 mM Hepes pH 7.4, 10 mM NaCl, 2 mM $MgCl_2$, with those predicted by Equation 4. Within the range of molecular dimensions studied, the depositions on freshly cleaved mica carried out in low salt buffer lead to adequate equilibration of the molecules on the surface. Moreover, the variance of the square of the end-to-end distance, $\sigma^2_{\vec{R}^2} = 2/3\langle\vec{R}^2\rangle^2$ (23), also agree quantitatively with the corresponding theoretical values predicted for molecules at equilibrium in two dimensions. In contrast, pretreatment of the mica surface by either glow discharge or monovalent salts yields end-to-end distance values less than those predicted by the equilibrium model. That different mechanisms of deposition operate in these two cases is confirmed by the different appearance of the DNA fragments on the mica observed in the two cases (Figure 5).

Another test of surface equilibrium of DNA molecules on mica can be obtained from the equilibrium distribution of bend angles between two DNA segments separated by a distance, ℓ, along the molecule. This distribution is predicted to be Gaussian by the wormlike and the "hinge" models of polymer statistics (39, 68). According to these models, the bending energy of the molecule in two dimensions is simply (39, 68)

$$E_{\text{bend}} = \frac{k_B T P \theta^2}{2\ell}, \qquad 5.$$

where k_B is the Boltzman constant, T is the absolute temperature, P is the persistence length of DNA, and θ is the bend angle spanning a length of arc ℓ. Although the standard deviation of the angle distribution in two dimensions can be written simply as

$$\langle\theta^2\rangle = \frac{\ell}{P}. \qquad 6.$$

Figure 6 shows a plot of the $\langle\theta^2\rangle$ values obtained from the SFM images of DNA fragments of different length deposited in low salt buffer on mica (C Rivetti, M Guthold, and C Bustamante, in preparation). For DNA molecules up to 1500 bp, the persistence length calculated from the slope of the plot is approximately 53 nm, in excellent agreement with values in the literature (12, 25). For longer fragments, the measured persistence length appears larger, probably because of excluded volume effects.

Bezanilla et al (5) recently presented evidence that DNA molecules partially bound to the mica by electrostatic interactions can equilibrate on the surface. These authors imaged DNA molecules under buffer

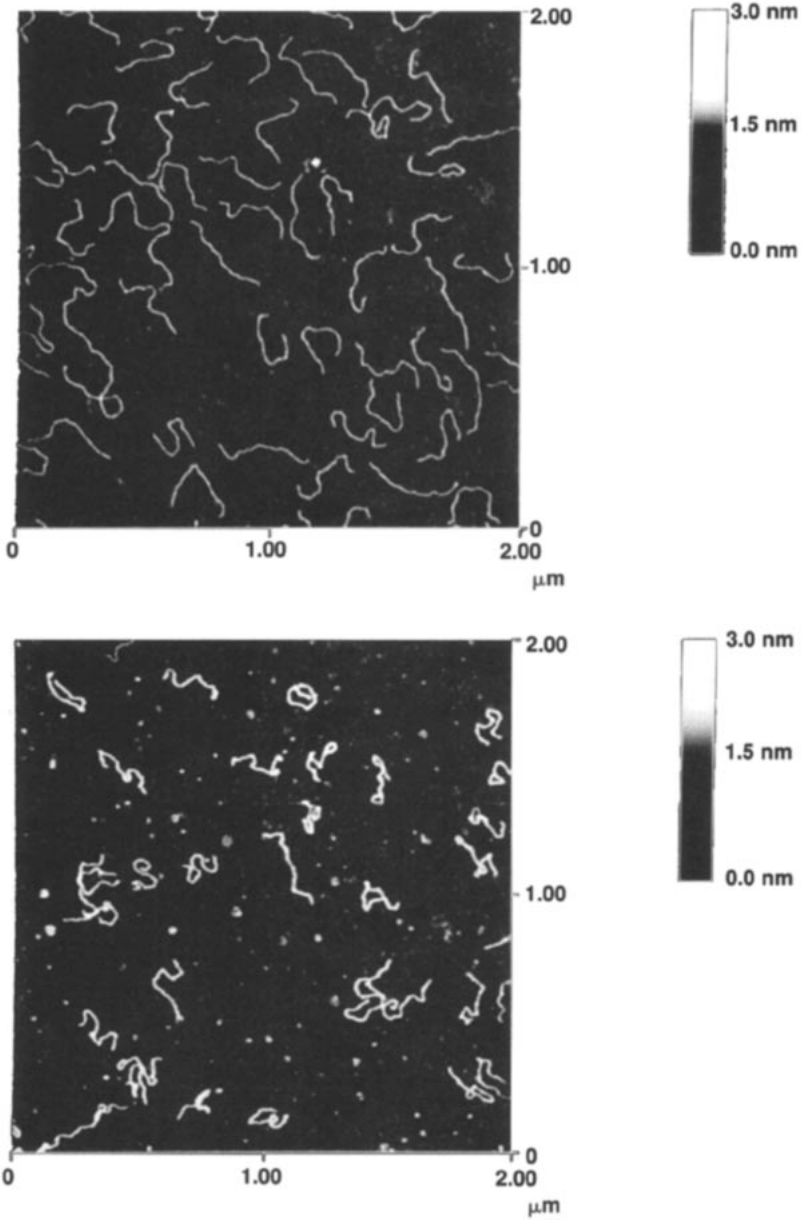

Figure 5 Atomic force microscopic images of a 1258-bp DNA fragment. *(top)* Twenty microliters of a 1 nM DNA solution in low salt buffer (10 mM Hepes pH 7.4, 10 mM NaCl, 2 mM $MgCl_2$) were deposited on freshly cleaved untreated mica and incubated for 2 min before the extra liquid was blotted and the surface was dried. *(bottom)* Twenty microliters of a 0.5 nM DNA solution in the same buffer were deposited on glow discharged mica and incubated for approximately 1 min. The mica disk was glow discharged in vacuum for 10 s.

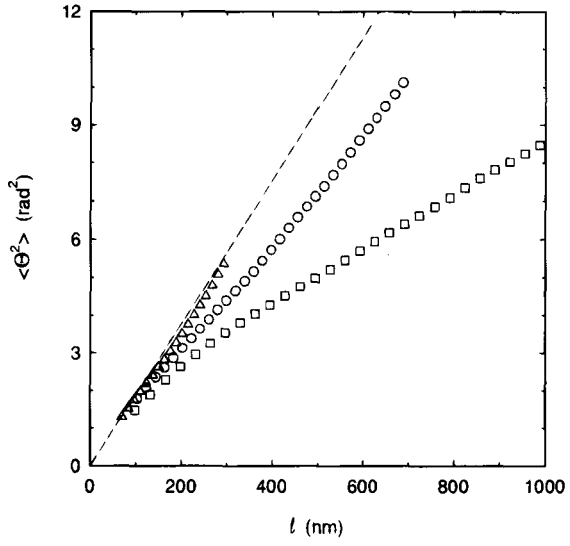

Figure 6 Plot of the mean square angle between two DNA segments as a function of their separation ℓ, for DNA fragments of three different lengths. The persistence length values obtained from the inverse of the slope of the regressions are: *triangles,* 1258 bp, $P = 55.1$ nm; *circles,* 2712 bp, $P = 71.1$ nm; *squares,* 5994 bp, $P = 144.5$ nm. DNA fragments shorter than 1000 bp behave like the 1258-bp fragments (data not shown). The apparent persistence length of the two longer fragments is higher probably caused by excluded volume effects. The DNA molecules were deposited and imaged as described in Figure 5.

that were deposited on mica surfaces treated with Ni^{++}. Under these conditions, they could observe the movement of some of the molecules on the surface. Similar results have been obtained with Mg^{++}-treated mica.

The results described above are likely to be applicable to protein–nucleic acid complexes, as long as the deposition process is dominated by the nucleic acid. Conversely, if the protein–mica interaction is stronger than the DNA–mica interaction, the mean square end-to-end distance of the protein-bound DNA should be smaller than the corresponding value for free DNA. An experiment to determine whether proteins bound to a DNA fragment can affect its equilibration on the mica surface has been performed recently (C Rivetti, M Guthold, and C Bustamante, in preparation). DNA fragments labeled at both bends with streptavidin were deposited in low salt buffer on mica, and their average end-to-end distance was determined by SFM and compared with that of free DNA deposited under identical conditions. The $\langle R^2 \rangle$

value of the streptavidin-labeled molecules was comparable to that of the free DNA. Some nucleic acid–binding proteins may interact more strongly with the mica surface than does streptavidin. Nonetheless, given the electrostatic nature of the molecule–surface interactions on mica, it is unlikely that the protein will dominate the deposition process or determine the global conformation of the complex.

This analysis shows that the strength of the molecule–surface interaction plays an essential role in the nature of the deposition process and its outcome. In general, as predicted by Equation 3, in the limit of strong molecule–surface interactions the deposition is "kinetic," i.e. any given part of the molecule that encounters the surface will remain bound to that location. If the energy of the surface interaction is any times greater than the energies holding the molecular assembly together, the process of deposition can easily alter the spatial relationships between the protein and the nucleic acid, promote complex dissociation, or induce the loss of native structures. In the limit of very weak surface interactions, however, equilibration in two dimensions is very likely, but the weak binding forces may lead to low deposition yield. Between these two extremes, there exists an intermediate range of interactions that result in a good yield of surface-equilibrated molecular depositions. Avoiding kinetic trapping effects is essential for the study of the global conformations of protein–nucleic acid complexes, particularly for the analysis of protein-induced DNA bending, as we discuss later. For these reasons, glow discharged mica or other surface pretreatments, such as monovalent salts, that lead to strong surface interactions should be avoided.

Thermodynamic and Kinetic Factors Affecting the Deposition of Protein–Nucleic Acid Complexes

Quantitative SFM analysis requires an adequate density of molecules on the surface. Optimal DNA surface coverage can be obtained by adjusting the concentration of the DNA in the deposition drop and the deposition time properly (Equation 2). As shown above, optimal deposition densities on mica result when DNA molecules are deposited at nanomolar concentrations with deposition times of 1–2 min. Obtaining optimal deposition densities of protein–nucleic acid complexes is more involved, however, because their concentration and deposition time cannot be varied arbitrarily. Instead, concentrations and time of deposition are constrained by the stability of the complex and by its lifetime.

The simplest equilibrium between a protein P and its DNA binding site D can be written as:

$$PD \Leftrightarrow P + D,$$

and its dissociation constant is given by:

$$K_{diss} = \frac{(R - r)(1 - r)[P_T]}{Rr},$$

where $R \equiv [P_T]/[D_T]$, P_T and D_T are the total concentrations of protein and specific DNA sites in the deposition drop, respectively, and r is the fraction of DNA specific sites occupied by the protein.

Under typical reaction conditions, $R \cup 1$, and half saturation of the DNA sites is obtained when the protein and DNA concentrations $[P_T] = [D_T] = 2K_{diss}$. Moderate to very stable protein–nucleic acid complexes (i.e. $K_{diss} = 10^{-9}$ M $- 10^{-13}$ M), can be deposited with high yield on mica at nanomolar concentrations with deposition times of 1–2 min. If the complexes are relatively unstable, however, (i.e. $K_{diss} = 10^{-6}$ M $- 10^{-7}$ M), similar reaction conditions will yield only 0.1 to 1% of the DNA sites occupied by the protein at equilibrium. Unfortunately, deposition at micromolar concentrations cannot be used, as they will result in excessive surface coverage even for very short deposition times. Likewise, ways to stabilize the complexes by the addition of BSA or of glycerol can seriously compromise the quality of the images and ultimately prevent the binding of the complexes to the surface. One way to overcome this problem is to carry out the binding reaction at concentrations near the dissociation constant of the complex and quickly dilute the sample to nanomolar concentrations before the deposition step. Clearly, the success of this approach will depend ultimately on the lifetime of the complex, τ. Long-lived complexes ($\tau > 5$ min) could be captured on the surface with this method, thereby improving the deposition yield. On the other hand, this approach usually fails for complexes with lifetimes of a few seconds or less, as these complexes tend to dissociate extensively during the 30 s or so minimally required for deposition, blotting, and rinsing. In the latter case, depositions could be carried out at lower temperatures to increase the lifetime of the complex, or the complex could be stabilized by cross-linking. Cross-linking should be considered only as a last resort, however, because it could affect the conformation of the complexes in an unpredictable manner.

PROBING PROTEIN–NUCLEIC ACID INTERACTIONS

During the last 3 years, the SFM has been used to characterize the geometry and the spatial relationships of several protein–nucleic acid

complexes. These studies have been directed to characterize the structure of specific and nonspecific protein-nucleic acid complexes (18, 26, 62, 90), determine the stoichiometry of the complexes (18, 85), probe local molecular conformations of DNA by use of specific antibodies (55), and follow protein–nucleic acid interactions in buffer (24).

The nucleoprotein complexes studied by SFM encompass a broad range of protein sizes, from large, multisubunit molecules, such as RNA polymerase ($M_r \sim 450$ kDa) (26, 62, 90), to small transcription regulatory proteins like Cro, which binds to DNA as a dimer ($M_r = 2 \times 7.6$ kDa) (18). This enormous range is mainly due to the extreme sensitivity of the SFM to variations in height and the ability of SFM to image nucleoprotein assemblies without external means of contrast.

Protein-Induced DNA Bending

Many cell processes are regulated by DNA-binding proteins that can bind to target sequences on the DNA with high affinity and specificity. Examples of these processes include transcriptional regulation, hormone receptor–mediated activation, and certain types of site-specific recombination. In the last 10 years, it has become clear that these strong, highly specific interactions use both direct and indirect readout mechanisms (17, 51, 78). Direct readout involves recognition of the nucleic acid sequence by an appropriate protein domain. The protein uses indirect readout, however, to probe the local conformation of the DNA molecule at or in the immediate vicinity of the cognate site. This mechanism exploits the sequence-dependent local conformation and mechanical properties of the nucleic acid molecule (16, 52, 72).

A particular DNA sequence may be considered capable of both adopting a preferred configuration (e.g. localized A conformations, localized B conformations, and bends) and having access to alternative conformations within a given energy range. In other words, the preferred conformation of the site, as well as its flexibility, is likely to play an important role in indirect readout mechanisms (78). Because the binding free energies associated with specific protein–nucleic acid interactions can be 15–30 times greater than the thermal energy, k_BT, both the protein and the nucleic acid can modify their conformation and attain a compromise of high affinity and specificity. Protein-induced DNA deformations, such as bending (15), overwinding (8, 37), and underwinding (7, 71), are common occurrence in protein–nucleic acid complexes and appear to be essential in a variety of gene expression processes and their regulation.

An increasing number of prokaryotic and eukaryotic transcription

factors have been found to bend the DNA on binding to their specific site (79). DNA bending can regulate transcription in several ways. It can bring distally bound transcription factors together, for example, by facilitating DNA looping. It could facilitate the proper orientation of protein factors relative to one another and relative to the promoter, thereby acting as a transcriptional switch (54). In addition, bending could be required for specific site recognition (18), or the energy stored in the protein-induced bend could facilitate initiation or maturation from initiation to elongation complexes (79).

DNA bending can be characterized by circular permutation analysis (84), phasing analysis (91), cyclization analysis (44, 70), rotational relaxation (57), and high-resolution microscopy (21, 22). One of the main advantages of high-resolution microscopy is that it makes it possible to determine not only mean bend angles but also the bend angle distributions. The shape of these distributions can give information about the flexibility of the protein–DNA complex, the existence of single or multiple populations in solution, and the conformational changes of the protein, the DNA, or both.

The bend angle is defined as the deviation of the DNA from linearity and can be measured as the supplement of the angle determined by the tangents of the DNA molecule at the entry and exit points from the protein. Alternatively, if the DNA fragment is not too long, the bend angle can be determined indirectly from its effect on the end-to-end distance distribution of the DNA fragment (27, 69).

ANALYSIS OF PROTEIN-INDUCED DNA BEND ANGLES: SURFACE EFFECTS

Structural characterization of protein–nucleic acid complexes by SFM is reliable only if the deposition process itself does not affect the conformation of the complexes. As discussed above, kinetic trapping effects can lead to surface-induced configurations easily. In particular, trapping of the DNA on the surface can result in modified bend-angle distributions, with altered means and standard deviations. Meaningful angle distributions, therefore, can be obtained only if the complexes are allowed to equilibrate on the surface during deposition.

The configuration of a complex in which the protein induces a simple bend in the nucleic acid is inherently two dimensional. In this simple case, it is possible to analyze the effect of the binding energy on the mean and the standard deviation of the angle distributions. The explicit angle-dependent energy of a complex in solution that has a mean angle $\langle \theta \rangle$ can be written as (C Walker, WA Rees, DA Erie, and C Bustamante, in preparation):

$$E^{\text{soln}}(\theta) = E^{\text{soln}}(\langle\theta\rangle) + \frac{1}{2}\frac{f^2E^{\text{soln}}(\theta)}{f\theta^2}\bigg|_{\theta=\langle\theta\rangle}(\theta - \langle\theta\rangle)^2 + \ldots$$

$$\Delta E^{\text{soln}}(\theta) = \frac{1}{2}\,\mathrm{k}(\theta - \langle\theta\rangle)^2 \qquad 7.$$

$$\mathrm{k} \equiv \frac{f^2E^{\text{soln}}(\theta)}{f\theta^2}\bigg|_{\theta=\langle\theta\rangle},$$

where k is the constant of bending rigidity of the complex. The probability distribution of angles θ adopted by the complex in solution is then:

$$P(\theta) = \sqrt{\frac{\mathrm{k}}{2\pi k_{\mathrm{B}}T}}\, e^{-\,\mathrm{k}(\theta-\langle\theta\rangle)^2/2\mathrm{k}_{\mathrm{B}}\mathrm{T}} \qquad 8.$$

and its standard deviation is $s = \sqrt{\dfrac{\mathrm{k}_{\mathrm{B}}T}{\mathrm{k}}}$.

For complexes in contact with a surface, an energy term that describes the interaction of the complex with the surface must also be included:

$$E^{\text{surf}} = E^{\text{soln}} + E^{\text{surf .int}}, \qquad 9.$$

and the value of the bending constant, k, must be multiplied by a factor of two to account for the loss of one degree of freedom. If the second term in Expression 9 is independent of the angle θ, its inclusion amounts only to a multiplicative factor in the angular distribution (Equation 8). In this case, the surface energy interaction will not affect the angular distribution. This situation is, in fact, the most likely one given the nonspecific, electrostatic nature of the complex–surface interaction. It is much less likely for the surface binding energy to depend on the bending angle. This analysis shows that, under the most likely scenario, equilibration should give rise to distributions that are unaffected in both their mean and their standard deviation.

The standard deviation of the distributions can provide information about the stiffness of the protein–nucleic acid complex. Because of the finite spatial resolution of the microscope, the tangents to the DNA at the entry and exit points in the complex must be obtained over finite DNA lengths. These tangents are subjected to fluctuations determined by the persistence length of the DNA and the DNA lengths (Equation 6). As a result, the variance of the bend angle distributions contains the contributions of the bending rigidity of the complex, σ_{c}, and that of the bending rigidity of the DNA arms, σ_{b}, i.e.:

$$\sigma^2 = \sigma_{\mathrm{c}}^2 + \sigma_{\mathrm{b}}^2 = \sigma_{\mathrm{c}}^2 + \frac{\ell}{P}. \qquad 10.$$

Using Equation 1 for a parabolic tip with a radius of curvature, R_c = 8 nm, a limit of detectability, Δz = 0.1 nm, and a height difference between the protein and the DNA, Δh = 0.4 nm, gives a DNA arm length, $\ell/2$ = 4 nm. Assuming a value of 53 nm for the persistence length of the DNA molecule, the second term in the above expression predicts a standard deviation, $\sigma = \sigma_b \sim 22^0$. Equation 11 shows that it is possible to obtain information about the rigidity of the protein–nucleic acid complex from the standard deviations of the population, if the contribution caused by the flexibility of the DNA can be estimated.

The analysis presented in this section assumes that the bent complexes are inherently two dimensional. If a protein can bend the DNA in two different locations, however, the bends generally will not be coplanar. Similarly, if the molecule induces torsion in at least one bending site, the result will again be a three-dimensional configuration determined by the individual bend angles and by the dihedral angle between the planes that contain the individual bends. In these cases, the deposition will always involve a transformation of a three-dimensional structure onto a two-dimensional surface. The interpretation of the data in this event can be extremely difficult.

DNA BENDING IN PROKARYOTIC TRANSCRIPTION COMPLEXES Several groups have reported transcription complexes of *Escherichia coli* RNA polymerase with various prokaryotic promoters, imaged in air by SFM (13, 62, 90). Images of open λ-P_L promoter complexes and stalled elongation complexes that harbor a 15-nucleotide long transcript revealed the large-scale morphology of the complexes and the spatial relationships between the polymerase and the DNA. Significantly, the DNA appears bent in both types of complexes (Figure 7*A* and *B*), but the elongation complexes are more severely bent (mean angle, 92°) than the open promoter complexes (mean angle, 54°). This difference appears to be related to the conformational changes associated with the maturation from open promoter complexes to elongation complexes (38, 50). An independent determination of the DNA bending in transcription complexes has been obtained with the use of electric birefringence (48). These studies reported a mean bend angle of 45° for open promoter complexes. In addition, complexes of *E. coli* RNA polymerase with supercoiled plasmids that contain the promoter of the ampicillin-resistance gene have been imaged with the use of SFM (90). The polymerase molecules often appear bound at the terminal loops of the plectonemes, a result consistent with polymerase-induced bending of the DNA.

DNA BENDING IN NONSPECIFIC COMPLEXES Direct visualization of protein–nucleic acid complexes makes it possible to characterize not only the conformation of the specifically bound proteins but also the conformations of the much less understood nonspecific interactions (18). Specific and nonspecific complexes can be distinguished and independently analyzed if the location of the specific site with respect to one end of the molecule is known. Nonspecific interactions are likely to play an important role in the processes of facilitated target location of their cognate site (4, 81). Moreover, practically all DNA binding proteins can also bind DNA nonspecifically; comparison between specific and nonspecific complexes, therefore, can provide important insight into the molecular basis of specificity. Recently, the conformation of specific and nonspecific Cro protein–DNA complexes has been characterized with the use of SFM. A DNA fragment containing the O_{R1}, O_{R2}, and O_{R3} sites of the O_R region of bacteriophage λ located four ninths from one end was used as template. The study revealed that Cro bends the DNA in specific (average bend angle, 69° ± 11°), as well as in nonspecific (average bend angle, 62° ± 23°), complexes. Figure 8 shows the distribution of DNA bend angles determined for nonspecific Cro–DNA complexes. This distribution suggests that bending the DNA at nonspecific sites may be an important component in the mechanism of specific site recognition by Cro. In other words, the protein may sample contacts needed for recognition of its target sequence via DNA bending. If Cro diffuses along the DNA in search of its operator (4, 81), the observed bending of nonspecific DNA would result in the propagation of a "bending wave" along the DNA with Cro riding at

Figure 7 (*A* and *B*) Surface plots of transcription complexes of *E. coli* RNA polymerase deposited on mica and imaged in air by using SFM in contact mode. *(A)* Open promoter complex (OPC); *(B)* elongation complex (C15). The DNA fragment (681 bp) contained the λ P_L promoter located four ninths from one end (62). *(C)* Surface plots of a three Cro dimers (*arrows*) bound to each of the operator sites in a 1-kbp DNA fragment containing the O_R region of bacteriophage λ. The complexes were deposited on mica and imaged in air by using SFM in tapping mode (18). *(D)* Line plot image of DNA-HSF2 complexes deposited on mica and imaged in air by using the tapping mode. The complex on the left shows a single HSF2 trimer (not resolved) bound to an HSE site positioned near the middle of the fragment. The complex on the right shows that two HSF2 trimers (each bound to a corresponding HSE site) are required to form the HSF2-mediated DNA loops associated with maximum transcription activation (85). (e) Line plot image of an NTRC protein (in front) interacting with *E. coli* RNA polymerase (in the back) via DNA looping to form an active transcription complex. The complexes were deposited on freshly cleaved mica and imaged in tapping mode in air. (Image courtesy of M Guthold and K Rippe, Institute of Molecular Biology, University of Oregon.)

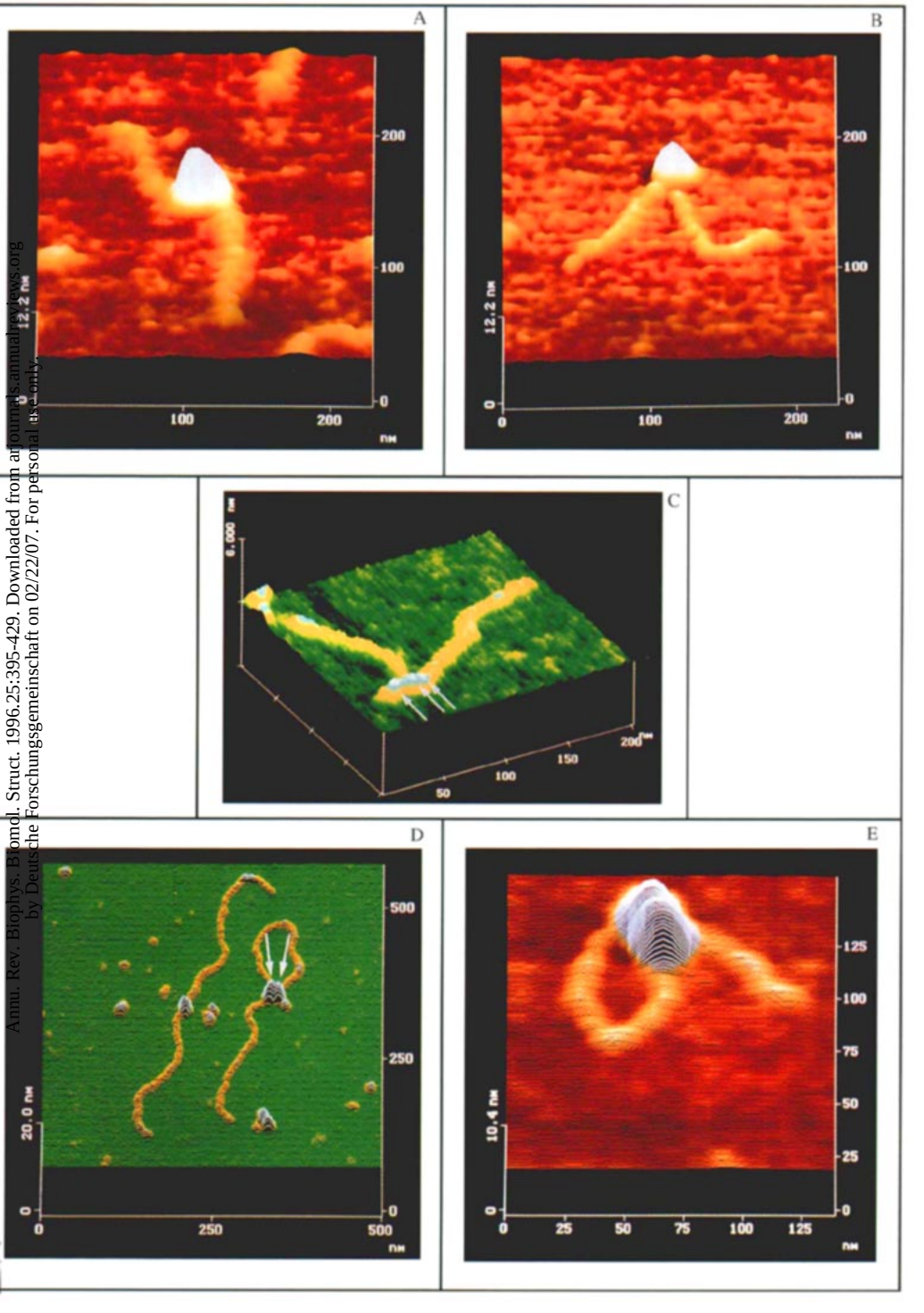

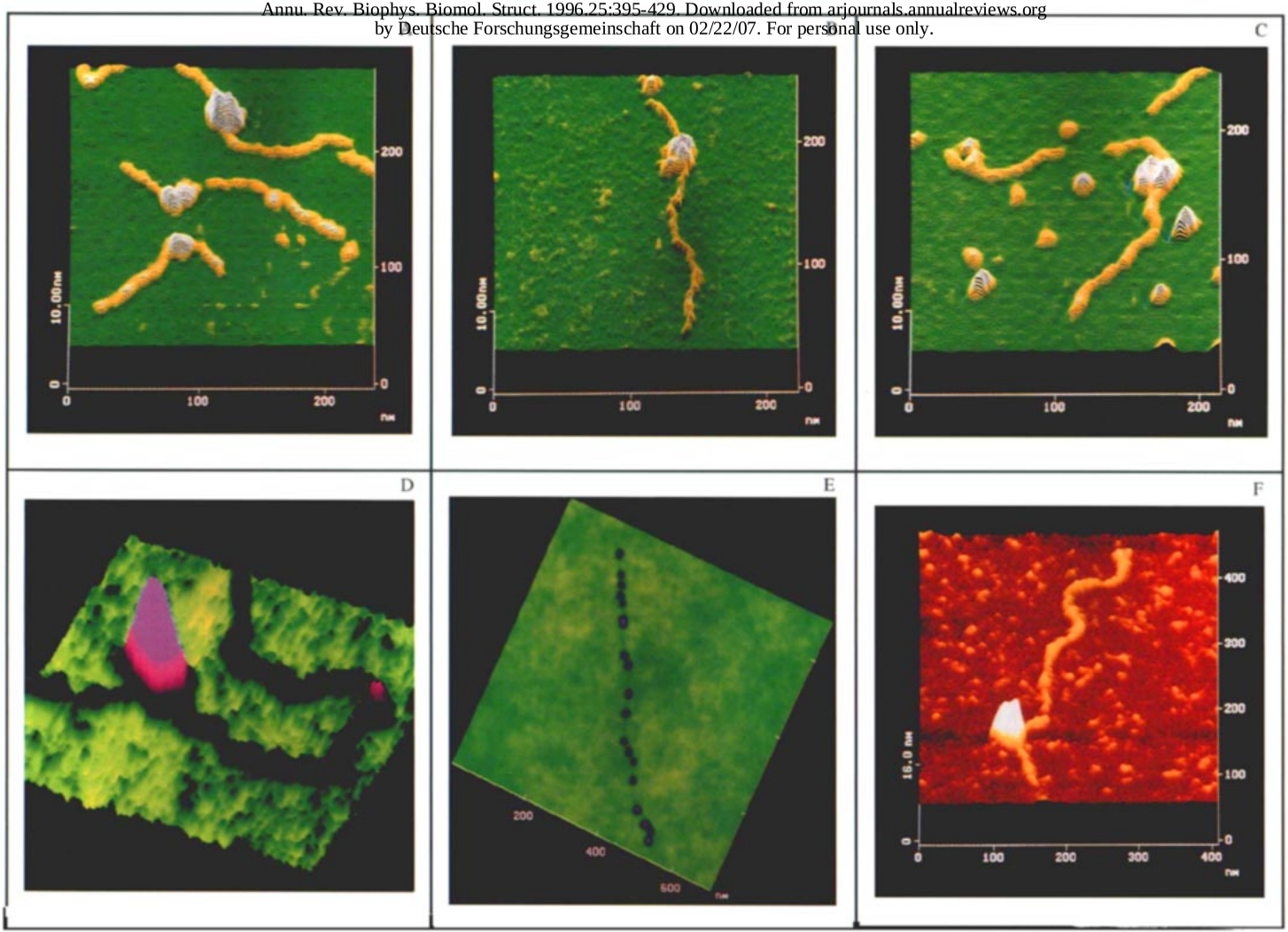

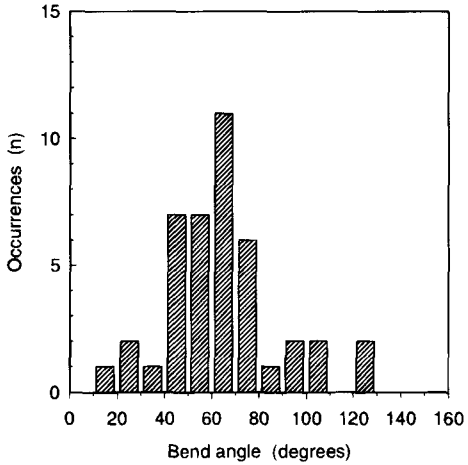

Figure 8 Histogram of the frequency of occurrence of DNA bend angles of nonspecific Cro–DNA complexes measured from SFM images. The mean value was 62° ± 23° (18).

its apex. The diffusion of the bending wave along the DNA can be shown to be energetically feasible (18).

COMPARISON TO OTHER METHODS Table 1 lists the values of the bend angles of various protein–nucleic acid complexes measured by SFM

Figure 10 *(A)* Line plot image of three different protein–nucleic acid complexes deposited on mica and imaged in air by using the tapping mode. (*bottom*) A complex of a single NTRC dimer (MW = 110 kDa) bound to a single enhancer element located in a 388-bp DNA fragment; (*middle*) a complex of two NTRC dimers (MW = 220 kDa) bound to a strong enhancer element located in a 610-bp DNA fragment; (*top*) an RNA polymerase (MW = 450 kDa) bound to a 1.8-kbp DNA fragment. *(B)* Line plot image of a complex of phosphorylated NTRC and a strong enhancer element. NTRC was phosphorylated in vitro by NTRB and ATP. *(C)* Line plot image of an unphosphorylated constitutive NTRC mutant (S160F NTRC) bound at a strong enhancer site. (From C Wyman, C Bustamante, and S Kustu, in preparation). *(D)* Surface plot of an IgG/Z-DNA complex obtained in air by using the tapping mode (55). (Image courtesy of L Pietrasanta and TM Jovin, Department of Molecular Biology, Max Planck Institute for Biophysical Chemistry.) *(E)* SFM image of linear DNA reconstituted with 18 core histones. The DNA contained a repeated DNA sequence that preferentially phases nucleosomes. The contour length of the chromatin fiber is 693 nm (1). (Image courtesy of MJ Allen, Department of Biological Chemistry, School of Medicine and Microbiology, University of California.) *(F)* SFM image of a stalled elongation complex of *E. coli* RNA-polymerase deposited on freshly cleaved mica and obtained under aqueous buffer in tapping mode with a carbon beam tip. The DNA fragment is 1258 bp long, and the stalling site is located one sixth from one end. (Image courtesy of XZ, Institute of Molecular Biology, University of Oregon.)

Table 1 Bend angle values of several DNA binding proteins obtained by different methods

Protein	Method			
	SFM[1]	Gel bend shift[2]	X-ray[3]	Others[4]
EcoRV[a]	43° ± 29	44°	50°	—
EcoRI endo[b]	10° ± 52	55°	12°	—
EcoRI MTase[c]	51° ± 17	50°	—	—
HhaI MTase[d]	2° ± 28	0°	0°	—
Cro[e]	69° ± 11	30°	40°	45°
RNAP[f]	54° ± 31	—	—	45°

[a1] Scanning force microscopy (SFM) on mica in air (C Walker, WA Rees, DA Erie, and C Bustamante, in preparation); [a2] circular permutation (73); [a3] X-ray (82). [b1] SFM on mica in air (C Walker, WA Rees, DA Erie, and C Bustamante, in preparation); [b2] circular permutation (75); [b3] X-ray (35, 47). [c1] SFM on mica in air (RA Garcia, C Bustamante, and NO Reich, in preparation); [c2] circular permutation (RA García, C Bustamante, and NO Reich, in preparation). [d1] SFM on mica in air (RA García, C Bustamante, and NO Reich, in preparation); [d2] circular permutation (RA García, C Bustamante, and NO Reich, in preparation); [d3] X-ray (36). [e1] SFM on mica in air (18); [e2] circular permutation (34); [e3] X-ray (8); [e4] ligase catalyzed cyclization (42). [f1] SFM on mica in air (62); [f4] electric birefringence (48).

and compares them with the corresponding values obtained by other methods (C Walker, WA Rees, DA Erie, and C Bustamante, in preparation). With the exception of EcoRI endonuclease, the values of the bend angles are in good agreement among the different methods of determination. The discrepancy concerning this protein likely reflects a complex interaction between the protein and the nucleic acid that is not described easily by a simple bend. In fact, the crystal structure indicates that EcoRI induces two phase bends on the DNA (35, 47). As noted above, how the measured angle would depend on the relative orientation of the three-dimensional structure, as it is projected on the surface, is not known.

Protein–Nucleic Acid Stoichiometry

Imaging of biological samples by SFM does not require any external means of contrast, and the spatial resolution of the SFM is limited only by the finite dimensions of the tip and the geometry of the sample (10). This fact makes the SFM particularly suited to visualize multiprotein–nucleic acid assemblies, determine their stoichiometry, and characterize their spatial relationships. Only a few systems have been studied to date; we review three cases here as illustration.

Figure 7*C* depicts a tapping mode image obtained in air of Cro protein molecules bound to the three operator sites in the O_R region of bacteriophage λ (18). Cro binds to each operator site as a dimer to repress

transcription from the divergent λ promoters P_R and P_{RM} (59). With a molecular weight of only 14.7 kDa, these dimers (the arrows point to each of three Cro dimers) are among the smallest proteins imaged by any kind of microscopy. The distance between each peak is 7.1 nm. The dimple depth between adjacent peaks is only 0.3 nm, but well within the height resolution of the instrument.

Another application of the SFM to determine the stoichiometry of protein–nucleic acid complexes is illustrated in Figure 7*D*. This image shows the loop structure induced in a DNA fragment by the human transcription activator heat shock factor 2 (HSF2). This factor activates transcription by binding to specific sites on the DNA, called heat shock elements (HSEs). These elements occur close and far from the promoter. At least one close HSE of three nGAAn repeats are necessary for transcription, whereas distally located HSEs function as transcriptional enhancers. This process often results in looped DNA structures bringing together one proximal and one distal HSE to contact the promoter, as shown in Figure 7*D*. Because each HSF2 binds to the HSE as a trimer (not resolved by the SFM), it was not known whether the loops required two HSF2 trimers (one bound to a distal HSE and the other bound to the proximal HSE), or if just one single trimer could effect the looping, as is found for AraC (41). Attempts to resolve this question by EM gave ambiguous results. Scanning force microscopic images obtained with the use of the tapping mode in air closely show the presence of two distinct and symmetrically bound peaks at the closure of the looped activation complex (85). Volume analysis of complexes at the loop junction relative to the HSF2 monomers confirmed that each peak corresponds to an unresolved HSF2 trimer (85).

Transcription initiation by σ^{54}RNA polymerase from *E. coli,* in response to conditions of nitrogen starvation, is controlled by protein factors bound to enhancer sequences far from the promoter, via DNA looping. This system might be considered a primitive analogue of transcription regulation at a distance, as seen often in eukaryotic systems (49). Transcription is activated in an ATP-dependent manner by nitrogen regulatory protein C (NTRC). This protein binds as a dimer (M_r = 110 kDa) to each of the two sites of an enhancer element that are located at -108 and -140 from the start site of transcription. Activation involves the isomerization reaction from close to open promoter complex and requires NTRC phosphorylation, a process carried out in vivo by the autokinase nitrogen regulatory protein B (NTRB) (58). At least two dimers in the complex are necessary for activation, and the function of the enhancer appears to be that of increasing the concentration of NTRC in the vicinity of the glnA promoter. The hypothesis that

phosphorylation may promote the formation of multiprotein complexes was postulated on the basis of electron micrographs of phosphorylated NTRC/enhancer complexes (74) and has been demonstrated recently with the use of SFM (C Wyman, C Bustamante, and S Kustu, in preparation). Figure 7*E* shows the looped structure of NTRC and σ^{54}RNA polymerase bound to a 726-bp DNA fragment that contains the glnA promoter and two tandemly arranged enhancer sites.

Determination of molecular weight of multiprotein–nucleic acid assemblies with the use of SFM is difficult because the heights of proteins and nucleic acids often appear smaller than their true values. There could be multiple causes for this situation, including denaturation of the molecules on binding to the surface, mechanical compliance of the molecules under the force exerted by the tip, and differential interaction of the tip with the molecule and the background. The underestimation of the molecular volume resulting from the flattening of the images is compensated, in part, by the overestimation of the lateral dimensions of the protein owing to the finite size of the tip. These two opposite effects may be responsible for the linear proportionality between molecular weight and the volume observed in the range of 110 to 500 kDa (Figure 9).

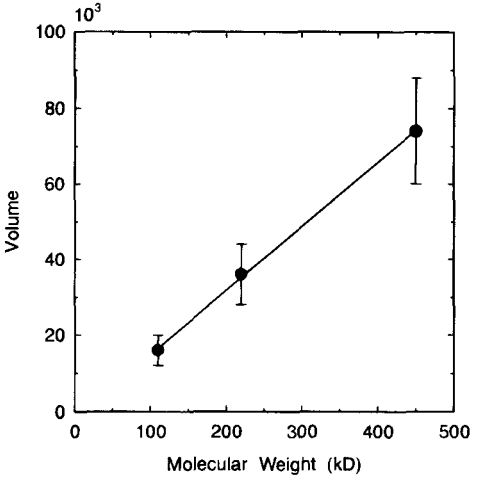

Figure 9 Molecular weight vs volume of three DNA-protein complexes imaged by SFM in air. The data were obtained by averaging 171 single NTRC dimers (MW = 110 kDa), 81 RNA polymerase molecules (MW = 450 kDa), and 123 double NTRC dimers (MW = 220 kDa) bound to specific DNA sequences. The volumes are expressed in arbitrary units, and the error bar represents the standard deviation from the mean for each complex. (From C Wyman, C Bustamante, and S Kustu, in preparation.)

Figure 10*A* shows a single unphosphorylated NTRC dimer bound to a 388-bp DNA fragment that contains a single enhancer element (*bottom*), two unphosphorylated dimers bound to a 610-bp fragment that contains two tandem enhancer elements (strong enhancer) (*middle*), and a molecule of RNA polymerase bound to a 1.8-kbp fragment that contains the λ P_R promoter (*top*). Figure 10*B*, shows the effect of phosphorylation on the binding of NTRC to the strong enhancer. Under these conditions, NTRC binds as a multimer of dimers. In fact, analysis of many complexes (C Wyman, C Bustamante, and S Kustu, in preparation) showed that 43% of the NTRC-enhancer complexes contain more than two NTRC dimers. For comparison, under identical conditions, only 2% of the unphosphorylated NTRC-enhancer complexes contained more than two NTRC dimers. Significantly, 34% of the complexes formed with a constitutive NTRC mutant (S160F) capable of transcription activation in the absence of phosphorylation contained more than two NTRC dimers (Figure 10*C*).

Conformation-Dependent Molecular Recognition: Immuno-SFM

Recently, an anti-Z DNA antibody was used to probe for the left-handed Z-DNA conformation of a $d(CG)^{11}$ insert in a negatively supercoiled DNA plasmid (55). The SFM images revealed that the antibody remained bound to the DNA even after the plasmids were cleaved with a restriction endonuclease (Figure 10*D*). The bound antibodies had apparent lateral dimensions of 35 nm and a height of 2 nm from the mica surface. The antibodies were often found in a lateral orientation relative to the DNA, an observation consistent with the previous data that indicated a bipedal mode of binding for an anti-Z-DNA IgG. The SFM images suggest that the DNA bends to accommodate the two Fab-combining regions of the antibody.

High-Order Protein–Nucleic Acid Assemblies: Chromatin Studies

Several groups have used the SFM to image whole sperm in buffer (2, 3, 30, 88). These authors have examined the contents of lysed sperm cells in air and in buffer and have shown the toroidal packing organization of the DNA in the nucleus (88). Recently, cell preparation methods from optical and electron microscopy were adapted and used successfully to image lysed cells with SFM in air and in buffer (19, 20).

Fibers of purified chicken erythrocyte chromatin imaged in air by SFM were shown to exhibit an irregular, three-dimensional arrangement of nucleosomes even at low ionic strength (9, 40, 93). The SFM

images closely resemble images recently obtained by cryo-electron microscopy of thin nuclear sections (83). Computer simulations carried out by these authors suggested that these three-dimensional irregular structures could result from the natural variability of the DNA linker lengths in chromatin fibers. Computer simulations can also reproduce most of the topographic features of the SFM images and suggest several of the factors that may be responsible for maintaining the integrity of these fibers in solution (86). Among these factors are the presence of the linker histones H1 and H5. Fibers stripped of these histones lack three-dimensional structures that display a "beads-on-a-string" appearance (86). Partially trypsinized chromatin fibers have been also imaged in air by SFM (92). Digestion of the N- and C-terminal domains of the linker histones did not affect the entry and exit angles of the DNA around the nucleosome. This result indicates that the presence of the globular domain of the linker histones is sufficient to maintain this angle in the fiber.

Studies with 21,000-bp *Tetrahymena thermophila* rDNA minichromosomes chromatin fibers recently have shown no less than a sixfold compaction of B-DNA into an irregular fiber, which appears to contain some zig zag regions (46).

Allen and coworkers (1) have studied linear and circular DNA reconstituted with the core histones but without the linker histones H1 and H5. Under these conditions, the reconstituted fibers depict a beads-on-a-string appearance (Figure 10*E*). Using a repeated DNA sequence that preferentially phases nucleosomes, these authors could titrate the eighteen positioning sites on the DNA fragment and characterize the resulting DNA compaction.

Following Protein–Nucleic Acid Interactions in Buffer

Perhaps the most exciting and promising application of the SFM is its ability to operate under liquids in close to physiologic conditions. Although only a few protein–nucleic acid complexes have been imaged in buffer, the following examples illustrate the potential of this capability, unique to the SFM.

Guthold et al (24) used the SFM to follow the assembly of *E. coli* RNA polymerase and DNA. These authors deposited molecules of DNA onto freshly cleaved mica and imaged them in contact mode under low salt aqueous buffer solutions before injecting a solution of RNA polymerase. They showed that it is possible to image the same area of the mica before and just 1 min after the injection of the polymerase. These authors recognized several molecules of RNA polymerase that had bound to the DNA molecules within this time. The results

demonstrate that the deposition conditions used could preserve the binding activity of the polymerase and that the presence of the surface does not interfere significantly with the binding process.

Figure 10*F* shows an image of an elongation complex of *E. coli* RNA polymerase and the λ P_R promoter. The molecules were deposited on mica and imaged under a low salt aqueous buffer in tapping mode. Successive images of these complexes showed various parts of the complexes moving somewhat on the mica surface. This observation suggests that it is possible to deposit the complexes with minimal attachment to the mica and to image them with SFM using the tapping mode in liquid. With this capability, it may be possible to use the SFM to visualize and follow in real time the processes of transcription and replication.

CONCLUDING REMARKS

Ten years have passed since the invention of the SFM (6). During this time, much progress has occurred in the development of the instrument and in the design and testing of protocols and methods to image biological samples. With a reliable performance and ease of operation, the ability to image macromolecules without external means of contrast, and the capacity to operate under aqueous solutions with nanometer resolution, the SFM is rapidly becoming a useful tool for structural studies of mesoscopic systems.

In addition to the current capabilities of the SFM reviewed here, a number of important challenges in the area of protein–nucleic acid interactions will soon be able to be addressed for the first time with this technique. For example, biochemists may soon learn how to take advantage of the SFM operation under liquids to follow in real time the assembly of increasingly larger nucleoprotein complexes, characterize their spatial relationships in physiologically relevant conditions, investigate their conformational changes on variations in solution conditions, and follow in real time their biochemical processes.

These efforts, aided by concurrent instrumental and technical developments, may play an important role in helping biochemists integrate the high-resolution and large-scale pictures into a comprehensive view of the mechanisms of control and regulation of transcription and replication.

ACKNOWLEDGMENTS

This work was supported by National Science Foundation grants MBC 9118482 and BIR 9318945 and National Institutes of Health grant GM-

32543. This work was supported in part by a grant from the Lucille P. Markey Foundation to the Institute of Molecular Biology. Claudio Rivetti was supported by a Human Frontier Science Program long-term fellowship.

Literature Cited

1. Allen MJ, Dong XF, O'Neill TE, Yau P, Kowalczykowski SC, et al. 1993. Atomic force microscope measurements of nucleosome cores assembled along defined DNA sequences. *Biochemistry* 32:8390–96
2. Allen MJ, Hud NV, Balooch M, Tench RJ, Siekhaus WJ, Balhorn R. 1992. Tip-radius-induced artifacts in AFM images of protamine-complexed DNA fibers. *Ultramicroscopy* 42–44: 1095–100
3. Allen MJ, Lee C, Lee JD IV, Pogany GC, Balooch M, et al. 1993. Atomic force microscopy of mammalian sperm chromatin. *Chromosoma* 102: 623–30
4. Berg OG, von Hippel PH. 1985. Diffusion-controlled macromolecular interactions. *Annu. Rev. Biophys. Biophys. Chem.* 14:131–60
5. Bezanilla M, Drake B, Nudler E, Kashlev M, Hansma PK, Hansma HG. 1994. Motion and enzymatic degradation of DNA in the atomic force microscope. *Biophys. J.* 67:2454–59
6. Binnig G, Quate CF, Gerber CH. 1986. Atomic force microscope. *Phys. Rev. Lett.* 56:930–33
7. Bramhill D, Kornberg A. 1988. A model for initiation at origins of DNA replication. *Cell* 52:743–55
8. Brennan RG, Roderick SL, Takeda Y, Matthews BW. 1990. Protein-DNA conformational changes in the crystal structure of a lambda Cro-operator complex. *Proc. Natl. Acad. Sci. USA* 87:8165–69
9. Bustamante C, Erie DA, Keller D. 1994. Biochemical and structural applications of scanning force microscopy. *Curr. Opin. Struct. Biol.* 4: 750–60
10. Bustamante C, Keller D. 1995. Scanning force microscopy in biology. *Phys. Today* 48:32–38
11. Bustamante C, Keller D, Yang G. 1993. Scanning force microscopy of nucleic acids and nucleoprotein assemblies. *Curr. Opin. Struct. Biol.* 3: 363–72
12. Bustamante C, Marko JF, Siggia ED, Smith S. 1994. Entropic elasticity of l-phage DNA. *Science* 265:1599–600
13. Bustamante C, Vesenka J, Tang CL, Rees W, Guthold M, Keller R. 1992. Circular DNA molecules imaged in air by scanning force microscopy. *Biochemistry* 3:22–26
14. Butt HJ, Muller T, Gross H. 1993. Immobilizing biomolecules for scanning force microscopy by embedding in carbon. *J. Struct. Biol.* 110:127–32
15. Crothers DM, Gartenberg MR, Shrader TE. 1991. DNA bending in protein-DNA complexes. *Methods Enzymol.* 208:118–46
16. Drew HR, McCall MJ, Calladine CR. 1988. Recent studies of DNA in the crystal. *Annu. Rev. Cell Biol.* 4:1–20
17. Drew HR, Travers AA. 1985. Structural junctions in DNA: the influence of flanking sequence on nuclease digestion specificities. *Nucleic Acids Res.* 13:4445–67
18. Erie DA, Yang G, Schultz HC, Bustamante C. 1994. DNA bending by Cro protein in specific and nonspecific complexes: implications for protein site recognition and specificity. *Science* 266:1562-66
19. Fritzsche W, Schaper A, Jovin TM. 1994. Probing chromatin with the scanning force microscope. *Chromosoma* 103:231–36
20. Fritzsche W, Schaper A, Jovin TM. 1995. Scanning force microscopy of chromatin fibers in air and in liquid. *Scanning* 17:148–55
21. Griffith JD, Makhov A, Zawel L, Reinberg D. 1995. Visualization of TBP oligomers binding and bending the HIV-1 and adeno promoters. *J. Mol. Biol.* 246:576–84

22. Gronenborn AM, Nermut MV, Eason P, Clore GM. 1984. Visualization of cAMP receptor protein-induced DNA kinking by electron microscopy. *J. Mol. Biol.* 179:751–57
23. Grosberg AY, Khokhlov AR. 1994. *Statistical Physics of Macromolecules*. Woodbury, NY: API. 350 pp.
24. Guthold M, Bezanilla M, Erie DA, Jenkins B, Hansma HG, Bustamante C. 1994. Following the assembly of RNA polymerase-DNA complexes in aqueous solutions with the scanning force microscope. *Proc. Natl. Acad. Sci. USA* 91:12927–31
25. Hagerman PJ. 1988. Flexibility of DNA. *Annu. Rev. Biophys. Biophys. Chem.* 17:265–86
26. Hansma HG, Bezanilla M, Zenhausern F, Adrian M, Sinsheimer RL. 1993. Atomic force microscopy of DNA in aqueous solutions. *Nucleic Acids Res.* 21:505–12
27. Hansma HG, Browne KA, Bezanilla M, Bruice TC. 1994. Bending and straightening of DNA induced by the same ligand: characterization with the atomic force microscope. *Biochemistry* 33:8436–41
28. Hansma HG, Hoh J. 1994. Biomolecular imaging with atomic force microscope. *Annu. Rev. Biophys. Biomol. Struct.* 23:115–39
29. Hansma PK, Cleveland JP, Radmacher M, Walters DA, Hillner P, et al. 1994. Tapping mode atomic force microscopy in liquids. *Appl. Phys. Lett.* 64:1738–40
30. Hud NV, Allen MJ, Downing KH, Lee J, Balhorn R. 1993. Identification of the elemental packing unit of DNA in mammalian sperm cell by atomic force microscopy. *Biochem. Biophys. Res. Commun.* 193:1347–54
31. Isrealachvili J. 1992. *Intermolecular and Surface Forces*. New York: Academic. 450 pp.
32. Keller D, Chou CC. 1992. Imaging steep high structures by scanning force microscopy with electron beam deposited tips. *Surf. Sci.* 268:333–39
33. Keller DJ, Franke FS. 1993. Envelope reconstruction of scanning probe microscope images. *Surf. Sci.* 294: 409–19
34. Kim J, Zweib C, Wu C, Adhyn S. 1989. Bending of DNA by gene-regulatory proteins: construction and use of a DNA bending vector. *Gene* 85: 15–23
35. Kim YC, Grable JC, Love R, Greene PJ, Rosenburg JM. 1990. Refinement of EcoRI endonuclease crystal structure: a revised protein chain tracing. *Science* 249:1307–9
36. Klimasauskas S, Kumar S, Roberts RJ, Cheng X. 1994. HhaI methyltransferase flips its target base out of the DNA helix. *Cell* 76:357–69
37. Koudelka GB, Harbury P, Harrison SC, Ptashne M. 1988. DNA twisting and the affinity of bacteriophage 434 operator for bacteriophage 434 repressor. *Proc. Natl. Acad. Sci. USA* 85: 4633–37
38. Krummel B, Chamberlin MJ. 1992. Structural analysis of ternary complexes of *Escherichia coli* RNA polymerase. Deoxyribonuclease I footprinting of defined complexes. *J. Mol. Biol.* 225:239–50
39. Landau LD, Lifshitz EM. 1986. *Theory of Elasticity*. Oxford, NY: Pergamon. 187 pp.
40. Leuba SH, Yang G, Robert C, Samorí B, van Holde K, et al. 1994. Three-dimensional structure of extended chromatin fibers as revealed by tapping-mode scanning force microscopy. *Proc. Natl. Acad. Sci. USA* 91: 11621–25
41. Lobell RB, Schleif RF. 1990. DNA looping and unlooping by AraC protein. *Science* 250:528–33
42. Lyubchenko YL, Jacobs BL, Lindsay SM. 1992. Atomic force microscopy of reovirus dsRNA: a routine technique for length measurements. *Nucleic Acids Res.* 20:3983–86
43. Lyubchenko YL, Oden PI, Lampner D, Lindsay SM, Dunker KA. 1993. Atomic force microscopy of DNA and bacteriophage in air water and propanol: the role of adhesion forces. *Nucleic Acids Res.* 21:1117–23
44. Lyubchenko YL, Shlyakhtenko L, Chernov B, Harrington RE. 1991. DNA bending induced by Cro protein binding as demonstrated by gel electrophoresis. *Proc. Natl. Acad. Sci. USA* 88:5331–34
45. Lyubchenko YL, Shlyakhtenko LS, Harrington RE, Oden PI, Lindsay SM. 1993. Atomic force microscopy of long DNA: imaging in air and under water. *Proc. Natl. Acad. Sci. USA* 90: 2137–40
46. Martin LD, Vesenka JP, Henderson E, Dobbs DL. 1995. Visualization of nucleosomal substructure in native chromatin by atomic force microscopy. *Biochemistry* 34:4610–16
47. McClarin JA, Frederick CA, Wang BC, Greene P, Boyer HW, et al. 1986. Structure of the DNA-EcoRI endonuclease recognition complex at 3

angstrom resolution. *Science* 234: 1526–41
48. Meyer-Alme FJ, Heumann H, Porschke D. 1994. The structure of the RNA polymerase-promoter complex: DNA bending by quantitative electrooptics. *J. Mol. Biol.* 236:1–6
49. North AK, Klose KE, Stedman KM, Kustu S. 1993. Prokaryotic enhancer-binding proteins reflect eukaryote-like modularity: the puzzle of nitrogen regulatory protein C. *J. Bacteriol.* 175: 4267–73
50. Nudler E, Goldfarb A, Kashlev M. 1994. Discontinuous mechanism of transcription elongation. *Science* 265: 793–96
51. Otwinowski Z, Schevitz RW, Zhang RG, Lawson CL, Joachimiak A, et al. 1988. Crystal structure of trp repressor/operator complex at atomic resolution. *Nature* 355:321–29
52. Pabo CO, Sauer RT. 1992. Transcription factors: structural families and principles of DNA recognition. *Annu. Rev. Biochem.* 61:1053–95
53. Pashley RM. 1981. Hydration forces between mica surfaces in aqueous electrolyte solutions. *J. Colloid Interface Sci.* 80:153–62
54. Pérez Martín J, Espinosa M. 1993. Protein-induced bending as a transcriptional switch. *Science* 260:805–7
55. Pietrasanta LI, Schaper A, Jovin TM. 1994. Probing specific molecular conformations with the scanning force microscope. Complexes of plasmid DNA and anti-Z-DNA antibodies. *Nucleic Acids Res.* 22:3288–92
56. Pingali GS, Jain R. 1992. Restoration of scanning force microscope images. In *Proc. IEEE Workshop on Appl. of Comput. Vision*, pp. 282–89
57. Porschke D, Hillen W, Tahahashi M. 1984. The change of DNA structure by specific binding of the cAMP receptor protein from rotation diffusion and dichroism measurements. *EMBO J.* 3: 2873–77
58. Porter S, North AK, Wedel AB, Kustu S. 1993. Oligomerization of NTRC at the glnA enhancer is required for transcriptional activation. *Genes Dev.* 7: 2258–73
59. Ptashne M. 1992. *A Genetic Switch: Phage* 1 *and Higher Organism.* Cambridge, MA: Blackwell Scientific. 192 pp.
60. Putman AJ. 1994. *In development of an atomic force microscope for biological applications.* PhD thesis. Univ. of Twente, Enschede
61. Putman AJ, Van der Werf KO, De Grooth BG, Van Hulst NF, Greve J. 1994. Tapping mode atomic force microscopy in liquid. *Appl. Phys. Lett.* 64:2454–56
62. Rees WA, Keller RW, Vesenka JP, Yang G, Bustamante C. 1993. Evidence of DNA bending in transcription complexes imaged by scanning force microscopy. *Science* 260:1646–49
63. Richmond TJ, Searles MA, Simpson RT. 1988. Crystals of a nucleosome core particle containing defined sequence DNA. *J. Mol. Biol.* 199: 161–70
64. Rugar D, Hansma PK. 1990. Atomic force microscopy. *Phys. Today* 43: 23–30
65. Sarid D. 1991. *Scanning Force Microscopy with Applications to Electric, Magnetic, and Atomic Forces.* New York: Oxford Univ. Press. 253 pp.
66. Schaper A, Pietrasanta LI, Jovin TM. 1993. Scanning force microscopy of circular and linear plasmid DNA spread on mica with a quaternary ammonium salt. *Nucleic Acids Res.* 21: 6004–9
67. Schaper A, Starink JP, Jovin TM. 1994. The scanning force microscopy of DNA in air and in n-propanol using new spreading agents. *FEBS Lett.* 355: 91–95
68. Schellman JA. 1974. Flexibility of DNA. *Biopolymers* 13:217–26
69. Schutz H, Reinert KE. 1991. DNA-bending on ligand binding: change of DNA persistence length. *J. Biomol. Struct. Dyn.* 9:315–29
70. Shore D, Langowski J, Baldwin RL. 1981. DNA flexibility studied by covalent closure of short fragments into circles. *Proc. Natl. Acad. Sci. USA* 78: 4833–37
71. Spassky A, Kirkegaard K, Buc H. 1985. Changes in the DNA structure of the lac UV5 promoter during formation of an open complex with *Escherichia coli* RNA polymerase. *Biochemistry* 24:2723–31
72. Steitz TA. 1990. Structural studies of protein-nucleic acid interaction: the sources of sequence-specific binding. *Q. Rev. Biophys.* 23:205–80
73. Stöver T, Köhler E, Fagin U, Wende W, Wolfes H, Pingoud A. 1993. Determination of the DNA bend angle induced by the restriction endonuclease EcoRV in the presence of Mg^{2+}. *J. Biol. Chem.* 268:8645–50
74. Su W, Porter S, Kustu S, Echols H. 1990. DNA-looping and enhancer activity: association between DNA-

bound NtrC activator and RNA polymerase at the bacterial glnA promoter. *Proc. Natl. Acad. Sci. USA* 87:5504–8
75. Thompson JF, Landy A. 1988. Empirical estimation of protein-induced DNA bending angles: applications to lambda site-specific recombination complexes. *Nucleic Acids Res.* 16: 9687–9705
76. Thundat T, Allison DP, Warmack RJ, Brown GM, Jacobson KB, et al. 1992. Atomic force microscopy of DNA on mica and chemically modified mica. *Scanning Microsc.* 6:911–18
77. Thundat T, Allison DP, Warmack RJ, Ferrel TL. 1992. Imaging isolated strands of DNA molecules by atomic force microscopy. *Ultramicroscopy* 42–44:1101–6
78. Travers AA. 1989. DNA conformation and protein binding. *Annu. Rev. Biochem.* 58:427–52
79. van der Vliet PC, Verrijzer CP. 1993. Bending of DNA by transcription factors. *BioEssays* 15:25–32
80. Vesenka J, Guthold M, Tang CL, Keller D, Delaine E, Bustamante C. 1992. Substrate preparation for reliable imaging of DNA molecules with the scanning force microscope. *Ultramicroscopy* 42-44:1243–49
81. von Hippel PH, Berg OG. 1989. Facilitated target location in biological systems. *J. Biol. Chem.* 264:675–78
82. Winkler FK, Banner DW, Oefner C, Tsernogl D, Brown RS, et al. 1993. The crystal structure of EcoRV endonuclease and of its complexes with cognate and non-cognate DNA fragments. *EMBO J.* 12:1781–95
83. Woodcock CL. 1994. Chromatin fibers observed in situ in frozen hydrated sections. Native fiber diameter is not correlated with nucleosome repeat length. *J. Cell Biol.* 125:11–19
84. Wu HM, Crothers DM. 1984. The locus of sequence-directed and protein-induced DNA bending. *Nature* 308:509–13
85. Wyman C, Grotkopp E, Bustamante C, Nelson HCM. 1995. Determination of heat-shock transcription factor 2 stoichiometry at looped DNA complexes using scanning force microscopy. *EMBO J.* 14:117–23
86. Yang G, Leuba SH, Bustamante C, Zlatanova J, van Holde K. 1994. Role of linker histones in extended chromatin fibre structure. *Nat. Struct. Biol.* 1: 761–63
87. Yang J, Takeyasu K, Shao Z. 1992. Atomic force microscopy of DNA molecules. *FEBS Lett.* 301:173–76
88. Zalensky AO, Allen MJ, Kobayashi A, Zalenskaya IA, Balhorn R, Bradbury EM. 1995. Well-defined genome architecture in the human sperm nucleus. *Chromosoma* 103:577–90
89. Zenhausern F, Adrian M, ten Heggeler-Bordier B, Emch R, Jobin M, et al. 1992. Imaging of DNA by scanning force microscopy. *J. Struct. Biol.* 108: 69–73
90. Zenhausern F, Adrian M, ten Heggeler-Bordier B, Eng LM, Descouts P. 1992. DNA and RNA Polymerase/DNA complex imaged by scanning force microscopy: influence of molecular-scale friction. *Scanning* 14: 212–17
91. Zinkel SS, Crothers DM. 1987. DNA bend direction by phase sensitive detection. *Nature* 328:178–81
92. Zlatanova J, Leuba SH, Bustamante C, van Holde KE. 1995. Role of the structural domains of the linker histones and histone H3 in the chromatin fiber structure at low-ionic strength: scanning force microscopy (SFM) studies on partially trypsinized chromatin. *SPIE Proc.* 2384:22–32
93. Zlatanova J, Leuba SH, Yang G, Bustamante C, van Holde K. 1994. Linker DNA accessibility in chromatin fibers of different conformations: a reevaluation. *Proc. Natl. Acad. Sci. USA* 91: 5277–80

Annual Review of Biophysics and Biomolecular Structure
Volume 25, 1996

CONTENTS